Title
Interstitial Optical Monitoring of Focal Laser Ablation.

Journal
IEEE Transactions on Biomedical Engineering, 69(8)

Authors
Geoghegan, Rory
Zhang, Le
Priester, Alan
et al.

Publication Date
2022-08-01

DOI
10.1109/TBME.2022.3150279

Peer reviewed

HHS Public Access

Author manuscript

IEEE Trans Biomed Eng. Author manuscript; available in PMC 2023 August 01.

Published in final edited form as:

IEEE Trans Biomed Eng. 2022 August ; 69(8): 2545–2556. doi:10.1109/TBME.2022.3150279.

Interstitial Optical Monitoring of Focal Laser Ablation

Rory Geoghegan [Member, IEEE],
Department of Urology, University of California Los Angeles, Los Angeles, CA 90095 USA.

Le Zhang,
Department of Radiology, Mayo Clinic

Alan Priester,
Department of Urology, University of California Los Angeles, Los Angeles, CA 90095 USA.

Holden H. Wu [Member, IEEE],
Department of Radiological Sciences, University of California Los Angeles.

Leonard Marks,
Department of Urology, University of California Los Angeles, Los Angeles, CA 90095 USA.

Shyam Natarajan [Member, IEEE]
Department of Urology, University of California Los Angeles, Los Angeles, CA 90095 USA.

Abstract

Focal laser ablation is a minimally invasive method of treating cancerous lesions in organs such as prostate, liver and brain. Oncologic control is achieved by inducing hyperthermia throughout the target while minimizing damage to surrounding tissue. Consequently, successful clinical outcomes are contingent upon achieving desired ablation volumes. Magnetic resonance thermometry is frequently used to monitor the formation of the induced thermal damage zone and inform the decision to terminate energy delivery. However, due to the associated cost and complexity there is growing interest in the development of alternative approaches. Here we investigate the utility of real-time interstitial interrogation of laser-tissue interaction as an inexpensive alternative monitoring modality that provides direct assessment of tissue coagulation without the need for organ specific calibration. The optical contrast mechanism was determined using a Monte Carlo model. Subsequently, four interstitial probe designs were manufactured and assessed in a tissue mimicking phantom under simultaneous magnetic resonance imaging. Finally, the optimal probe design was evaluated in ex vivo bovine muscle. It was found to be capable of providing sufficient feedback to achieve pre-defined ablation radii in the range 4–7mm with a mean absolute error of 0.3mm. This approach provides an inexpensive monitoring modality that may facilitate widespread adoption of focal laser ablation.

Index Terms—

laser; ablation monitoring; optical fiber sensors; oncology

rory.geoghegan@ucla.edu .

I. INTRODUCTION

Focal laser ablation (FLA) is a minimally invasive approach for the treatment of soft tissue tumors and has been used in many organs including prostate [1]–[3], breast [4], liver [5], lung [6] and brain [7]. During FLA, a laser fiber is inserted into the target tumor and oncologic control is achieved via thermally induced coagulative necrosis. Successful treatment is contingent upon inducing coagulative necrosis throughout the target volume while minimizing damage to surrounding healthy tissue. When the laser is activated, the coagulation zone initially forms around the fiber and then expands outwards. The physician is tasked with deciding when to terminate laser exposure. A similar decision is encountered in radiofrequency ablation (RFA) [8] and microwave ablation (MWA) [9]. These modalities are much more commonly used and the exposure duration is often chosen based on guidelines provided by device manufacturers [10]. This ‘one size fits all’ approach can be effective when overtreatment is possible; however, wide margins are often not feasible when tumors present adjacent to sensitive structures or where preservation of healthy tissue is critical. For example, in prostate cancer ablation, accurate control of ablation is critical to ensure oncologic control while avoiding damage to the neurovascular bundles and rectal wall which result in erectile dysfunction and rectal fistula respectively [11]. Similarly, it is highly desirable to preserve as much healthy tissue as possible when treating metastatic cancerous lesions in the lung and liver as multiple recurring lesions are frequently encountered [12]. Overtreatment may cause substantial organ impairment while undertreatment results in failure to achieve oncologic control.

Preservation of sensitive structures is also critical in neurosurgical applications where FLA has been adopted because in contrast to RFA and MWA, fiber optics are inherently compatible with magnetic resonance imaging (MRI); thus, enabling monitoring via magnetic resonance thermometry (MRT) [13]. MRT provides a near real-time 2D thermal map which is used to assess tissue damage and warn the operator if sensitive structures approach lethal temperatures. This approach has been used for monitoring ablation of lesions in numerous organs including brain [14], liver [15], and prostate [16]. For example, in a recent study, FLA was performed on 120 men with prostate cancer and monitored with MRT [17]. The mean procedure time was 122 minutes and follow-up biopsies identified residual clinically significant prostate cancer in 15% of patients. While the clinical results are promising, the high cost and extended treatment times associated with MRI present a major barrier to the widespread use of MRT. Additionally, MRT requires relatively long acquisition times which results in considerable motion artefact when imaging moving organs [13]. Consequently, there is a growing interest in the development of interstitial probes. Our group [18] and Lindner et al. [19] utilized commercially available fluoroptic thermal probes for monitoring FLA of prostate cancer. These probes provide a single point thermal measurement and are positioned at the desired ablation boundary with acquired data used to inform the decision to terminate laser exposure. Schena et al. improved on this approach by integrating an array of fiber Bragg grating thermal sensors into a single probe [20]. A similar probe has been commercialized by Novian Health (IL, U.S.A) with a recent clinical trial reporting complete ablation in 84% of breast cancer cases [21].

Given that FLA achieves oncologic control through hyperthermia, thermal monitoring appears appropriate; however, raw thermal data are of limited utility. Instead thermal data are generally used in conjunction with the Arrhenius thermal damage model which estimates cell death based on the magnitude and duration of hyperthermia [3], [22], [23]. Tissue specific kinetic parameters are also required inputs for the model but have proven to be difficult to quantify. Indeed, due to the variation in estimated kinetic parameters, the Arrhenius model may be inherently inaccurate when monitoring FLA [24]–[27]. The Arrhenius model has been found to overestimate the extent of thermal necrosis when compared to histopathology and T1-weighted contrast enhanced MRI [28]. In addition, the United States Food and Drug Administration issued a product recall for one MRT monitoring system (Visualase, Medtronic, Ireland) in 2018 due to inaccurate estimation of thermal damage during FLA [29]. Consequently, there is a need to either improve existing thermal damage models or develop alternative methods that do not require such models. A detailed outline of the myriad of techniques under investigation for thermal ablation monitoring can be found in Geoghegan et al. [30].

Here we outline the development and validation of an interstitial optical monitoring system that provides real-time feedback based on interrogation of laser-tissue interaction during FLA. In contrast to thermal monitoring, the proposed approach does not rely on a damage model that requires accurate knowledge of tissue parameters. Additionally, the change in optical properties is persistent thus enabling identification of coagulated tissue even after cooling which is not possible using a thermal monitoring approach. Inferring tissue damage from optical properties has also been recently explored using hyperspectral imaging; however, that approach is not suitable for percutaneous applications as it requires direct visualization of the organ surface [31], [32]. In this manuscript, we initially utilize Monte Carlo modelling to simulate FLA and identify a potential method of detecting the coagulation boundary. The performance of four optical probe designs is then assessed empirically in a novel study using a tissue mimicking phantom [33]. The phantom is designed with thermal and optical properties matched to prostatic tissue and facilitates visualization of the growth of the coagulation zone via customized dynamic T_2-weighted MRI scans. The data acquired here enable the development of an algorithm for ensuring complete coagulation of the target tissue. The optimal probe design and algorithm are subsequently validated in ex vivo bovine muscle by demonstrating the ability to achieve predefined coagulation radii.

II. METHODS

A. Simulation of Laser-Tissue Interaction

In FLA, oncologic control is achieved through thermally induced coagulative necrosis. A laser fiber with a diffuser on the distal end is used to deliver near-infrared light to deep lying interstitial targets. Photons are emitted from the diffuser, travel through the tissue, and ultimately deposit their energy when absorbed by chromophores. This process is governed by two wavelength specific tissue parameters: coefficient (μ_a) and the reduced scattering: coefficient (μ_s'). The distance that light travels into tissue before absorption is characterized by the effective penetration coefficient which is given as [34]:

$$\delta_{eff} = \frac{1}{\mu_{eff}}$$

with the effective attenuation coefficient defined by: $\mu_{eff} = \sqrt{3\mu_a(\mu_a + \mu_s')}$. In tissues with a long penetration depth, light is distributed over a large volume while the opposite occurs if the penetration depth is short.

A Monte Carlo simulation was used to investigate the impact of the expanding coagulation zone on the fluence that could potentially be recorded by interstitial optical probes during FLA [35]. The tissue structure was defined as a 2.5cm x 2.5cm x 2.5cm cube with a bin size of 0.005cm x 0.005cm x 0.005cm. To simplify the simulation, the diffuser was modeled as a single isotropic point source at the center of the cube surrounded by a spherical coagulation zone. The optical properties were matched to prostatic tissue at 980nm, specifically those of the tissue mimicking phantom which was also used for the subsequent in vitro experiment [33]. In the native tissue, μ_a and μ_s' were 0.66cm^{-1} and 8.27cm^{-1} respectively, with μ_s' in the spherical coagulation zone increased to 17.63cm^{-1}. An initial simulation was undertaken with no coagulation zone followed by 50 further simulations with coagulation radii ranging from 0.2–10mm in steps of 0.2mm. Each simulation used 8×10^5 photon packets. The fluence distributions from each simulation were then compiled together resulting in a large array, fluence = [x, y, z, r_c], where x, y and z are the spatial co-ordinates, and r_c is the coagulation radius. As the simulation is spherically symmetric (up to the maximum ablation radius of 10mm), this was further simplified to two dimensions, fluence = [r, r_c], where r is the spatial co-ordinate measured from the isotropic point source. Ultimately, this dataset enables the user to position a virtual sensor at any arbitrary region of interest and observe the signal that would be recorded as the coagulation zone forms.

B. Optical Monitoring System & In Vitro Evaluation

An optical monitoring system was designed, constructed, and evaluated in a tissue mimicking phantom. As depicted in Fig. 1a, light collected by the interstitial probe is transmitted to an amplified photodetector (PDA36A, Thorlabs, NJ, U.S.A.) using an SMA905 connector. The photodetector outputs an analog signal in the range 0–10V. Analog to digital conversion is performed by a microcontroller, Arduino Leonardo (Arduino LLC, Italy), at 1Hz. The microcontroller operates with a maximum voltage of 5V; therefore, a voltage divider is used to reduce the analog output range from the photodiode to 0–5V. Data from the microcontroller is transferred in real-time to a computer via USB. The computer runs in-house developed software (Python) which enables real-time collection, visualization, and analysis of the recorded photovoltage (V_p).

A total of four interstitial optical probes were designed, manufactured, and evaluated (Fig. 1b). The primary difference between probes lies in the range of angles over which they collect light. The isotropic probe consists of a 5m long, 200μm core optical fiber with the tip encased in a 20mm polycarbonate cap (Pioneer Optics, CT) which is press-fit into a carbon fiber tube. The polycarbonate cap contains titanium dioxide powder to scatter incoming light and thus enable isotropic light collection. The probe is designed to be MR safe to facilitate

testing under MRI. In addition, the diameter of the probe is similar to the 13Ga (outer diameter =2.413mm) flexi-needle used in a previous FLA clinical trial at our institution [18]. In contrast to the isotropic probe, the ballistic and backscatter probes only collect light from one side of the fiber with the former collecting light travelling away from the source and the latter detecting photons that have travelled beyond the probe and then scattered back towards the source. The final probe, designated ‘radial’, accepts light from all angles perpendicular to the long-axis of the probe.

To our knowledge, it is not possible to visualize the growth of the coagulation zone in vivo with current medical imaging technology. We have overcome this limitation by testing the optical monitoring system in a tissue mimicking phantom under simultaneous MRI. The phantom mimics both the thermal and optical properties of prostatic tissue at 980nm as outlined in Geoghegan et al. [33]. It is manufactured from polyacrylamide and the optical properties are modified by the addition of Naphthol Green B (Sigma-Aldrich, MI, N7257–100G), Intralipid (Fresenius Kabi, Sweden) and bovine serum albumin (CF-0020, Boval Co., TX, U.S.A). The coagulation zone is visible on MRI as thermal energy coagulates proteins in the phantom which reduce the protein-proton transverse relaxation time; thus, facilitating contrast between native and coagulated tissue on T_2-weighted MRI.

For each test, FLA was performed at 13.75W for 3 minutes as in our previous clinical trial [18]. Phantoms were placed in thin-walled plastic bags, preheated to body temperature using a water bath and then transferred to the insulated testing rig (Fig. 1c). The interstitial optical probes were tested at radial distances of 4mm, 5mm, 6mm and 7mm and simultaneously monitored with 3T MRI (Prisma, Siemens). This range was chosen as in-house testing found that coagulation radii greater than 7mm are difficult to achieve. The imaging plane was aligned along the trajectory of the laser fiber and the optical probe using water-filled fiducials that are visible in the transverse and sagittal images acquired by the MRI localizer. A T_2-weighted turbo spin echo sequence was then acquired to confirm correct alignment (PRE). Once confirmed, a customized dynamic version of this scan (INTRA) was used to monitor the growth of the coagulation zone during FLA. To ensure rapid image acquisition a trade-off was made between the signal to noise ratio (SNR), resolution and scan time. The computer used to record the photovoltage was positioned in the control room and the INTRA scan was subsequently temporally registered to this data via a manual timestamp. After laser deactivation, another high-quality scan was acquired (POST) using the same imaging parameters as the PRE scan. Table 1 outlines the key parameters of each MRI scan. The duration for each image of the INTRA scans is considerably shorter than the PRE/POST sequence due to a shorter echo time (TE), a shorter repetition time (TR) and a larger pixel size. In an effort to increase the SNR, the slice thickness was also increased relative to the PRE/POST scan.

C. Ex Vivo Validation

This study was undertaken as a pre-clinical validation of the ballistic probe design which was identified as the optimal design in the previous section. The goal was to assess the ability of real-time optical monitoring to achieve pre-defined coagulation radii in the range 4–7mm.

As described in Fig. 2, ex vivo bovine muscle samples were placed in 3D printed sample holders which compress the pliable tissue and facilitate accurate slicing along the laser fiber trajectory post FLA. Each sample holder was then placed in a water-proof bag and preheated to 37°C using a water bath for ~45 minutes. The sample holder was then transferred to an insulated testing rig with channels for laser fiber and optical probe insertion. FLA was performed at 980nm with a power of 13.75W and terminated upon detection of the photovoltage inflection point. The inflection point was found in real-time by a custom software package (Python) which quantifies the rate of change of photovoltage $\left(\frac{dV_p}{dt}\right)$ by fitting a second order polynomial to the most recent 10s of data and calculates the first derivative at the last recorded datapoint. Complete coagulation is indicated by an inflection point which is defined as $\frac{dV_p}{dt} \geq 0$ after observing $\frac{dV_p}{dt} < 0$.

After FLA, samples were placed in a freezer overnight and then sliced along the trajectory of the laser fiber using a deli slicer. After allowing samples to thaw for approximately 20 minutes, the coagulation zone was photographed (Canon, EOS Rebel) using a lightbox to ensure consistent lighting between samples

III. RESULTS

A. Simulation of Laser-Tissue Interaction

A Monte Carlo simulation was used to investigate the impact of the expanding coagulation zone on the photovoltage that could potentially be recorded by interstitial optical probes at known distances from the laser fiber (Fig. 3a) The model simulates FLA at 980nm in prostatic tissue; however, similar results can be expected for other soft tissues. Prior to the onset of coagulation, photons travel throughout the tissue with fluence decreasing as the distance from the source increases. The growth of the coagulation zone serves to trap photons closer to the source thus decreasing fluence outside the coagulation boundary (Fig. 3b). This occurs because protein coagulation alters laser-tissue interaction by increasing μ_s' while μ_a remains relatively constant [36], [37]. Consequently, coagulated tissue exhibits a decreased δ_{eff} and effectively acts as a ‘light trap’. This is generally considered a primary disadvantage of FLA as it limits the size of the ablation zone. However, here we aim to utilize real-time analysis of this phenomenon as a feedback mechanism to achieve desired coagulation volumes. Fig. 3c shows the fluence recorded by virtual sensors positioned in the range 4–7mm from the isotropic point source. This range was chosen based on prior clinical experience [18] in which it was difficult to achieve coagulation radii greater than 7mm while small ablation zones (r_c<4mm) were of limited utility. The data presented show that in each case, fluence decreases as the coagulation boundary expands towards the virtual sensor with an inflection point occurring as the coagulation boundary passes the sensor. This suggests that clinically, it may be possible to achieve coagulation zones of a pre-defined size by placing an interstitial optical probe at the desired coagulation boundary and terminating laser exposure upon observation of the inflection point

This Monte Carlo model simplifies the laser-tissue interaction that occurs during FLA; thus, substantial empirical evidence is necessary to fully illustrate the utility of interstitial optical measurements.

B. Optical Monitoring System & In Vitro Evaluation

Fig. 4a illustrates the effect of FLA induced coagulation on the photovoltage recorded by the ballistic probe positioned 5mm from the laser fiber. Dynamic MRI frames (INTRA) were acquired at ~0.5Hz and the coagulation boundary was delineated retrospectively using an in-house image analysis algorithm. The first image shown was acquired immediately after laser activation. Both the dual lumen catheter and optical probe are visible and the ablation zone has yet to form. In the second image, the ablation zone has formed and is expanding towards the optical probe while the photovoltage has begun to decrease. The coagulation zone is ellipsoidal in shape as the ablation was performed with a 15mm-long cylindrical diffuser. The next image shows that as the ablation zone reaches the probe, an inflection point is observed in the photovoltage data. Further growth of the coagulation zone has a minimal impact on the photovoltage as the ballistic probe is designed to only interrogate laser-tissue interaction between the laser source and the probe. The optical properties in this region have already changed to their coagulated state; thus, minimal change in photovoltage is observed even though the final image shows the ablation boundary extending beyond the optical probe.

The image analysis algorithm used here defines the threshold between native and coagulated pixels such that it minimizes the error between the coagulation boundary in the final INTRA scan and the higher resolution POST scan (Fig. 4b). In the POST scan, both the signal-to-noise ratio and spatial resolution are noticeably improved in comparison to the images in Fig. 4a as it was not necessary to optimize the imaging parameters for rapid image acquisition (see Table 1). Finally, temporal registration of the photovoltage (acquired at 1Hz) with the coagulation radii requires quantification of the ablation radius (from INTRA MRI frames acquired at ~0.5Hz) as a function of time which was achieved with a logarithmic fit for each ablation (r^2>0.92) as depicted in Fig. 4c.

All four interstitial optical probes were tested for a range of laser fiber to optical probe separations (r) of 4–7mm. The results shown in Fig. 5a (top row) illustrate that propagation of the coagulation boundary is characterized by a decrease in photovoltage with an inflection point observed once the boundary reaches the optical probe. This trend approximates the Monte Carlo simulation performed in the previous section. The backscatter probe placed 4mm from the laser fiber presents a notable exception as no substantial decrease in photovoltage is observed before the inflection point. These data support the hypothesis that the passing of the coagulation zone can be identified as an inflection in the optical signal. To assess the utility of this approach, the instantaneous rate of change of photovoltage $\left(\frac{dV_p}{dt}\right)$ was retrospectively quantified and its relationship to the coagulation radius is shown in Fig. 5a (bottom row). By observation, it is clear that a real-time feedback algorithm can be developed which identifies propagation of the coagulation zone towards the optical probe as $\frac{dV_p}{dt} < 0$ with complete coagulation signified by $\frac{dV_p}{dt} = 0$.

Retrospective analysis was performed to determine the coagulation radius that would have been achieved if the proposed feedback algorithm had been used to determine the laser deactivation time (for all probes except the backscatter probe at r=4mm). To assess the accuracy of each probe, the feedback algorithm derived coagulation radius was compared to the true radius as defined by the MRI data (Fig. 5b). All four optical probes were capable of identifying the passing of the ablation boundary with the mean absolute error ranging from 0.25mm to 0.39mm (Fig. 5c). An accuracy of approximately 1mm is highly desirable to ensure complete ablation of target tumors while preserving surrounding structures e.g., rectal wall during FLA of prostate cancer.

In this study, each optical probe consists of a single optical fiber; however, clinically it would be ideal to utilize a multielement probe capable of detecting light at predefined locations along the length of the probe. For example, when treating prostate cancer, it is critical that the rectal wall remains free from thermal damage. With a multielement optical probe, a single probe could be used to simultaneously monitor both the rectal wall and the intended coagulation boundary. It may also be advantageous to combine thermal and optical sensors into a single probe. In both cases, only the ballistic and backscatter designs can be easily integrated into a single probe or mounted on the outside of a rigid needle as they only require line of sight at a single point. In contrast, the addition of extra elements would block some of the light that would otherwise be collected by the isotropic and radial probes. Consequently, the ballistic probe was chosen as the optimum design as the backscatter probe does not exhibit the characteristic signal decrease when placed close to the laser fiber.

C. Ex Vivo Validation

The ability of the ballistic probe to achieve coagulation zones of a pre-defined radius was assessed by performing FLA in ex vivo bovine muscle. Fig. 6a shows the results from a set of experiments including the photovoltage recorded in real-time (top row), photographs of the ablation zone (middle row) and the pixel intensity along a profile line which was used to determine the coagulation radius (bottom row). For each image, the threshold pixel value between native and coagulated pixels is determined from all other images in the dataset (N=19) and then applied to the image under analysis.

The utility of optical monitoring is demonstrated in Fig. 6b which compares the measured ablation radius against the target ablation radius. The target ablation radius is the position of the probe relative to the laser fiber as the proposed protocol for achieving a predefined radius is to place the optical probe at the desired margin. As expected, there is a strong linear relationship between the measured ablation radius and the target ablation radius (r^2 =0.91). The absolute error (mean ± SD) was 0.3±0.1mm which is similar to that observed during the in vitro test.

Finally, we compare the requisite laser exposure duration for a given coagulation radius in ex vivo bovine muscle, the tissue mimicking phantom and in vivo human prostate (Fig. 6c). The exposure duration for the phantom was interpolated from the experiments in the previous section in which we derived the coagulation radius as a function of time. Consequently, it does not account for growth of the coagulation zone after the laser is deactivated; however, this error is expected to be minimal due to rapid cooling. The human

prostate data are taken from a previous clinical trial at our institution in which ten men received FLA followed by an MRI to assess the extent of coagulation based on non-perfused tissue [18]. In that study, overlapping ablation zones prevented measurement of individual ablations in all but one case. While the thermal and optical properties of the ex vivo bovine muscle were not measured, we can infer that they are substantially different to the tissue mimicking phantom and prostate by noting that there is a significant difference ($p<0.01$, Wilcoxon rank-sum) in the exposure time required to achieve coagulation radii greater than 5mm. In contrast, the requisite exposure duration to achieve an ablation radius of 7.5mm is similar in the phantom and in vivo studies.

IV. DISCUSSION

In FLA, a laser fiber is inserted into a target tumor and oncologic control is achieved through thermally induced coagulative necrosis. A successful treatment results in the destruction of the cancerous lesion and the preservation of surrounding healthy tissue. In many cases, treatment with a wide margin is not possible due to the presence of nearby sensitive structures (e.g. rectal wall in prostate) or the need to preserve healthy tissue to permit further intervention for recurring tumors (e.g. metastatic lung cancer). Consequently, real-time treatment monitoring is highly desirable. Currently, development has primarily focused on thermal monitoring modalities. MRT has seen some adoption but widespread use is limited due to the high associated cost and limited availability. Numerous studies have also evaluated the utility of interstitial thermal probes for monitoring ablation [18], [19], [21]. However, both MRT and thermal probes must be used in conjunction with a thermal damage model to convert temperature to cell death. The Arrhenius model is generally used but it requires knowledge of tissue specific kinetic parameters which are difficult to derive resulting in uncertainty in damage estimation.

Here, we have presented an alternative monitoring modality, interstitial optical monitoring, which leverages the unique characteristics of FLA. During FLA, thermally induced tissue coagulation alters tissue optical properties thus providing a contrast mechanism for monitoring ablation. Specifically, the sensor presented here is inserted in parallel to the laser fiber and detects the coagulation boundary in real-time as an inflection in the instantaneous rate of change of the recorded photovoltage. As demonstrated in the Monte Carlo simulation (Fig. 3), this inflection point occurs because coagulated tissue exhibits an increased μ_s'; therefore, δ_{eff} decreases as the coagulation boundary expands towards the probe and ultimately reaches a steady state once all of the tissue between the source and the probe has been coagulated. As the coagulation zone expands beyond the probe, some photons will be scattered backwards resulting in an increase in signal.

Four interstitial optical probes were designed and evaluated in a tissue mimicking phantom: 1) Isotropic – collects light from all angles, 2) Ballistic – only collects light travelling from source fiber towards optical probe, 3) Backscatter – only collects light that travels past the optical probe and is subsequently scattered backwards, and 4) Radial – collects light from all angles perpendicular to the probe. For each probe, the characteristic inflection in the optical signal was observed as the coagulation boundary reached the sensor (Fig. 5a). The only exception was the backscatter probe which when placed 4mm from the laser fiber exhibited

only a minimal decrease in signal with a sharp increase observed once the coagulation boundary passed 3.5mm. Indeed, in all cases only a minimal decrease in signal was observed during the initial growth of the coagulation radius (<3mm). Further propagation of the coagulation zone results in a sharp change in photovoltage; thus, indicating that the optical signal is dependent on optical interactions throughout a volume of material. Consequently, in addition to detecting the coagulation boundary, optical probes detect the initial formation of the coagulation zone around the laser fiber and its subsequent expansion. In contrast, an interstitial thermal probe only records the temperature of tissue under direct contact.

Retrospective analysis of the acquired photovoltage indicated that the instantaneous rate of change of the photovoltage (Fig. 5b) can be used to detect the coagulation boundary for probes placed 4–7mm from the source. This range was chosen because it was difficult to achieve coagulation radii greater than 7mm and is not a limitation of the optical monitoring approach itself. All four optical probe designs exhibited similar performance with the mean absolute error ranging from 0.25mm to 0.39mm.

As each probe design performed similarly, the optimal design was chosen based on manufacturing considerations. In contrast to the isotropic and radial probes, the ballistic and backscatter probes only require line of sight between the optical fiber and the tissue at a single point. This is advantageous as it allows bundling of multiple fibers in a single probe thus enabling optical detection along the length of the probe. Additionally, the fibers can be mounted on the outside of a rigid needle. Consequently, the ballistic probe was chosen as the optimal design because the signal detected by the backscatter probe at 4mm did not exhibit the anticipated decrease in photovoltage during the onset of coagulation.

With the ballistic probe identified as the optimal design, further testing was undertaken to assess the ability of the optical monitoring system to ensure a desired ablation radius. Ex vivo bovine muscle was chosen as it is readily available and unlike the tissue mimicking phantom, the optical and thermal properties are unknown and likely to vary between samples. Moreover, ex vivo bovine muscle has been used in similar studies analyzing the effect of thermally induced coagulation on tissue properties [38]–[40]. The accuracy of the interstitial optical monitoring system was assessed by comparing the measured coagulation radius against the target coagulation radius. The absolute error (mean ± SD) was found to be 0.3±0.1mm which is similar to that observed in the tissue mimicking phantom experiments. While the thermal and optical properties of the ex vivo bovine muscle were not measured, we can infer that they are substantially different to the tissue mimicking phantom (and thus prostate) by noting that there is a significant difference ($p<0.01$) in the exposure time required to achieve coagulation radii greater than 5mm (Fig. 6c). This confirms that in contrast to thermal monitoring (with the Arrhenius damage model), an optical monitoring approach can accurately identify the coagulation boundary without prior knowledge of tissue parameters as long as ablation induces a substantial increase in μ_s'.

In contrast to other methods of monitoring optical properties, this approach provides sufficient feedback to achieve ablation sizes of pre-defined size regardless of tissue type. Early work by Whelan et al. attempted to correlate the magnitude of the change in fluence with onset of coagulation during FLA [41]. Similarly, Anderson et al. monitored diffuse

reflectance during RFA and noted that ablation causes an increase in reflectance intensity at multiple wavelengths [42]. Spliethoff et al. improved on this work by correlating the change in spectral shape (reflectance across a range of wavelengths) with tissue coagulation [43]. None of these studies demonstrated the ability to achieve pre-defined coagulation radii, likely because these methods are sensitive to subtle changes in tissue type as well as tissue-probe coupling. Additionally, there is no obvious method of visualizing the growth of the ablation zone while simultaneously recording sensor information. Consequently, these studies note a change in optical signal during ablation but cannot directly correlate it with the coagulation boundary. We solved this problem using a tissue mimicking phantom and a dynamic MRI scan specifically designed to visualize growth of the ablation zone.

These results provide strong evidence in support of the optical monitoring system; however, a key limitation of the experimental approach must be considered. Specifically, in the ex vivo study, the image analysis algorithm used to determine the coagulation radius defines the coagulation threshold such that it minimizes the overall error. This threshold is determined from a dataset that does not include the image under analysis; however, it is possible that the true absolute error is greater than reported here. For example, if the optical monitoring system tends to underestimate the extent of ablation, the resulting bias is removed by the image analysis algorithm. However, the advantage of the algorithm over visual assessment is that measurement errors tend be systematic i.e. if the algorithm underestimates the ablation radius in one image by 1mm, then it underestimates the radius in all images by approximately 1mm. For this reason, we have also shown that there is strong linear relationship between the measured damage radius and the target damage radius (r^2 =0.91). While considerable effort was undertaken to ensure accurate measurement of the ablation radius, further work should be undertaken utilizing histological assessment. In addition, simultaneous thermal and optical monitoring could be undertaken to facilitate a direct comparison between both modalities.

Finally, the system was designed to improve upon the thermal monitoring approach employed in an earlier clinical trial [18]. As with the thermal monitoring approach, the ablation zone is assumed to be cylindrically symmetric around the laser fiber. This assumption may not be valid in all clinical scenarios particularly in close proximity to large blood vessels which act as heat sinks. It is therefore expected that treatment planning will serve a vital role in identifying the appropriate position for the laser fiber and sensor. Additionally, it may be useful to insert multiple probes to account for asymmetric tissue perfusion as demonstrated by De Vita et al. with interstitial thermal probes [44].

The development of a reliable, low cost, easy to use monitoring modality is a necessary prerequisite to the widespread adoption of FLA for oncologic applications. In this manuscript, we have demonstrated the utility of an interstitial optical monitoring system under the same conditions as a previous clinical trial. In comparison to thermal monitoring, the primary advantages of this optical monitoring system are: (1) prior knowledge of tissue parameters is not required, (2) tissue condition can be assessed before, during and after hyperthermia, and (3) both the onset and propagation of the coagulation zone can be tracked. By combining this technology with ultrasound guidance, it may be possible to perform FLA in the clinic rather than the MRI suite. It is envisioned that the resulting decrease

in procedure cost and complexity will facilitate adoption of FLA in numerous oncologic applications.

V. CONCLUSION

In conclusion, this manuscript presents an interstitial optical monitoring system capable of providing sufficient feedback to achieve coagulation zones of a desired size regardless of tissue type. In contrast to conventional thermal monitoring modalities, tissue specific damage models are not required and the persistent change in optical properties also facilitates identification of coagulated tissue after cooling.

ACKNOWLEDGMENT

This work was supported in part by the Jean Perkins Foundation and the U.S. National Cancer Institute (R01CA218547). L.M., S.N., and A.P. own equity in and/or receive salary from Avenda Health (Santa Monica, CA).

REFERENCES

[1]. Natarajan S et al. , “Focal Laser Ablation of Prostate Cancer: Phase I Clinical Trial.,” J. Urol, vol. 196, no. 1, pp. 68–75, 2016. [PubMed: 26748164]

[2]. Lindner U et al. , “Image guided photothermal focal therapy for localized prostate cancer: phase I trial.,” J. Urol, vol. 182, no. 4, pp. 1371–1377, 2009. [PubMed: 19683262]

[3]. Oto A et al. , “MR Imaging – guided Focal Laser Ablation for Prostate Cancer : Phase 1 Trial,” Radiology, vol. 267, no. 3, pp. 932–640, 2013. [PubMed: 23440319]

[4]. Haraldsdottir KH et al. , “Interstitial laser thermotherapy (ILT) of breast cancer,” Eur. J. Surg. Oncol, vol. 34, no. 7, pp. 739–745, 2008. [PubMed: 18291614]

[5]. Dick EA et al. , “MR-guided laser thermal ablation of primary and secondary liver tumours,” Clin. Radiol, vol. 58, no. 2, pp. 112–120, 2003. [PubMed: 12623039]

[6]. Rosenberg C et al. , “Laser Ablation of Metastatic Lesions of the Lung: Long-Term Outcome,” Am. J. Roentgenol, vol. 192, no. 3, pp. 785–792, 2009. [PubMed: 19234278]

[7]. Carpentier A et al. , “Real-time magnetic resonance-guided laser thermal therapy for focal metastatic brain tumors,” Neurosurgery, vol. 63, no. 1 SUPPL., pp. 21–29, 2008.

[8]. Han K et al. , “A single-center retrospective analysis of periprocedural variables affecting local tumor progression after radiofrequency ablation of colorectal cancer liver metastases,” Radiology, vol. 298, no. 1, pp. 212–218, 2020. [PubMed: 33170105]

[9]. Ruiter SJS et al. , “Liver microwave ablation: a systematic review of various FDA-approved systems,” Eur. Radiol, vol. 29, no. 8, pp. 4026–4035, 2019. [PubMed: 30506218]

[10]. Vogl TJ et al. , “Microwave ablation therapy: Clinical utility in treatment of pulmonary metastases,” Radiology, vol. 261, no. 2, pp. 643–651, 2011. [PubMed: 22012906]

[11]. Ahdoot M et al. , “Contemporary treatments in prostate cancer focal therapy,” Curr. Opin. Oncol, vol. 31, no. 3, pp. 200–206, 2019. [PubMed: 30865133]

[12]. Abtin F et al. , “Updates on current role and practice of lung ablation,” J. Thorac. Imaging, vol. 34, no. 4, pp. 266–277, 2019. [PubMed: 31094898]

[13]. Winter L et al. , “Magnetic resonance thermometry: Methodology, pitfalls and practical solutions,” Int. J. Hyperth, vol. 32, no. 1, pp. 63–75, 2016.

[14]. Lagman C et al. , “Laser neurosurgery : A systematic analysis of magnetic resonance-guided laser interstitial thermal therapies,” J. Clin. Neurosci, vol. 36, pp. 20–26, 2017. [PubMed: 27838155]

[15]. Anzidei M et al. , “Magnetic resonance-guided focused ultrasound ablation in abdominal moving organs: a feasibility study in selected cases of pancreatic and liver cancer,” Cardiovasc. Intervent. Radiol, vol. 37, no. 6, pp. 1611–1617, 2014. [PubMed: 24595660]

[16]. Chin JL et al. , “Magnetic Resonance Imaging–Guided Transurethral Ultrasound Ablation of Prostate Tissue in Patients with Localized Prostate Cancer: A Prospective Phase 1 Clinical Trial,” Eur. Urol, vol. 70, no. 3, pp. 447–455, 2016. [PubMed: 26777228]

[17]. Walser E et al. , “Focal Laser Ablation of Prostate Cancer : Results in 120 Patients with Low- to Intermediate-Risk Disease,” J. Vasc. Interv. Radiol, vol. 30, no. 3, pp. 401–409.e2, 2019. [PubMed: 30819483]

[18]. Natarajan S et al. , “Focal Laser Ablation of Prostate Cancer: Feasibility of Magnetic Resonance Imaging-Ultrasound Fusion for Guidance,” J. Urol, vol. 198, no. 4, pp. 839–847, 2017. [PubMed: 28396184]

[19]. Lindner U et al. , “Image guided photothermal focal therapy for localized prostate cancer: phase I trial.,” J. Urol, vol. 182, no. 4, pp. 1371–1377, 2009. [PubMed: 19683262]

[20]. Schena E et al. , “Solutions to improve the outcomes of thermal treatments in oncology: Multipoint temperature monitoring,” IEEE J. Electromagn. RF Microwaves Med. Biol, vol. 2, no. 3, pp. 172–178, 2018.

[21]. Schwartzberg B et al. , “Phase 2 Open-Label Trial Investigating Percutaneous Laser Ablation for Treatment of Early-Stage Breast Cancer : MRI, Pathology, and Outcome Correlations,” Ann. Surg. Oncol, vol. 25, no. 10, pp. 2958–2964, 2018. [PubMed: 29987603]

[22]. McNichols RJ et al. , “MR Thermometry-Based Feedback Control of Laser Interstitial Thermal Therapy at 980 nm,” Lasers Surg. Med, vol. 34, no. 1, pp. 48–55, 2004. [PubMed: 14755424]

[23]. Eggener SE et al. , “Phase II Evaluation of Magnetic Resonance Imaging Guided Focal Laser Ablation of Prostate Cancer,” J. Urol, vol. 196, no. 6, pp. 1670–1675, 2016. [PubMed: 27449263]

[24]. Bhowmick P et al. , “In vitro assessment of the efficacy of thermal therapy in human benign prostatic hyperplasia.,” Int. J. Hyperthermia, vol. 20, no. 4, pp. 421–439, 2004. [PubMed: 15204522]

[25]. Rylander MN et al. , “Measurement and mathematical modeling of thermally induced injury and heat shock protein expression kinetics in normal and cancerous prostate cells.,” Int. J. Hyperthermia, vol. 26, no. 8, pp. 748–764, 2010. [PubMed: 20858083]

[26]. He X and Bischof JC, “The kinetics of thermal injury in human renal carcinoma cells,” Ann. Biomed. Eng, vol. 33, no. 4, pp. 502–510, 2005. [PubMed: 15909656]

[27]. Walsh LP et al. , “In Vitro Assessment of the Efficacy of Thermal Therapy in Human Renal Cell Carcinoma,” Urology, vol. 70, no. 2, pp. 380–384, Aug. 2007. [PubMed: 17826524]

[28]. Bomers JGR et al. , “MRI-guided focal laser ablation for prostate cancer followed by radical prostatectomy: correlation of treatment effects with imaging,” World J. Urol, vol. 35, no. 5, pp. 703–711, 2016. [PubMed: 27541586]

[29]. U.S. Food and Drug Adminstration, “Class 2 Device Recall Visualase Thermal Therapy System,” 2018..

[30]. Geoghegan R et al. , “Methods of Monitoring Thermal Ablation of Soft Tissue Tumors – A Comprehensive Review,” Med. Phys, 2021.

[31]. De Landro M et al., “Hyperspectral Imagery for Assessing Laser-Induced Thermal State Change in Liver,” 2021.

[32]. De Landro M et al., “Prediction of In Vivo Laser-Induced Thermal Damage with Hyperspectral Imaging Using Deep Learning,” pp. 1–19, 2021.

[33]. Geoghegan R et al. , “A tissue-mimicking prostate phantom for 980 nm laser interstitial thermal therapy,” Int. J. Hyperth, vol. 36, no. 1, pp. 993–1002, 2019.

[34]. Welch AJ et al., Optical-thermal response of laser-irradiated tissue, vol. 2. New York: Springer, 2011.

[35]. Wang L and Jacques SL, “Monte Carlo Modeling of Light Transport in Multi-layered Tissues in Standard C,” Univ. Texas, MD Anderson Cancer Cent, pp. 4–11, 1992.

[36]. Roggan A et al., “Experimental setup and Monte-Carlo model for the determination of optical tissue properties in the wavelength range 330–1100nm,” in Proc. SPIE 2323, 1995, vol. 2323, pp. 21–36.

[37]. Nau WH et al. , “Measurement of thermal effects on the optical properties of prostate tissue at wavelengths of 1,064 and 633nm,” Lasers Surg. Med, vol. 24, no. 1, pp. 38–47, 1999. [PubMed: 10037350]

[38]. Whelan WM et al. , “A novel strategy for monitoring laser thermal therapy based on changes in optothermal properties of heated tissues,” Int. J. Thermophys, vol. 26, no. 1, pp. 233–241, 2005.

[39]. Jaywant S et al., “Temperature-dependent changes in the optical absorption and scattering spectra of tissues: correlation with ultrastructure,” in Laser-Tissue Interaction IV, 1993, vol. 1882, pp. 218–229.

[40]. Wu T et al. , “Assessment of Thermal Tissue Ablation With MR Elastography,” Magn. Reson. Med, vol. 45, no. 1, pp. 80–87, 2001. [PubMed: 11146489]

[41]. Whelan WM et al. , “A Novel Strategy For Monitoring Laser Thermal Therapy Based on Changes in Optothermal Properties of Heated Tissues,” Int. J. Thermophys, vol. 26, no. 1, pp. 835 233–241, 2005.

[42]. Anderson CD et al. , “Real-time spectroscopic assessment of thermal damage: Implications for radiofrequency ablation,” J. Gastrointest. Surg, vol. 8, no. 6, pp. 660–669, 2004. [PubMed: 15358325]

[43]. Spliethoff JW et al. , “Monitoring of tumor radio frequency ablation using derivative spectroscopy,” J. Biomed. Opt, vol. 19, no. 9, p. 097004, 2014.

[44]. De Vita E et al., “Fiber Optic Sensors-Based Thermal Analysis of Perfusion-Mediated Tissue Cooling in Liver Undergoing Laser Ablation,” vol. 68, no. 3, pp. 1066–1073, 2021.

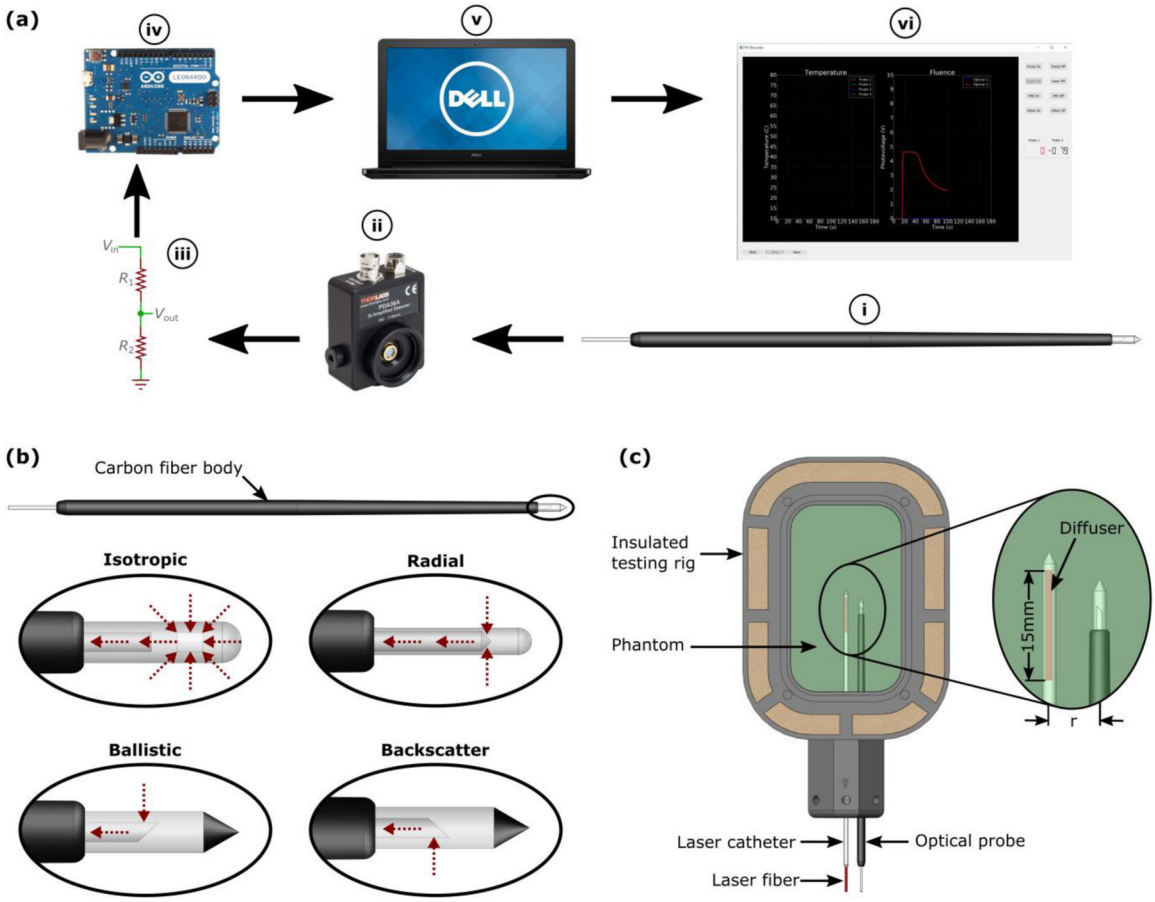

Fig. 1.

(a) Optical monitoring system in which light is collected at the distal tip of the interstitial probe (i) and transmitted along an optical fiber to an amplified photodetector (ii). The output voltage is reduced from 0–10V to 0–5V via a voltage divider (iii) and converted to a digital signal using a microcontroller (iv). The digital signal is read by a dedicated computer (v) running custom designed software (vi). (b) Detailed view of the four interstitial optical probe designs. Note, red arrows indicate directionality of light acceptance. (c) The experimental setup which was designed to match the clinical scenario where both the laser catheter and optical probe are inserted in parallel

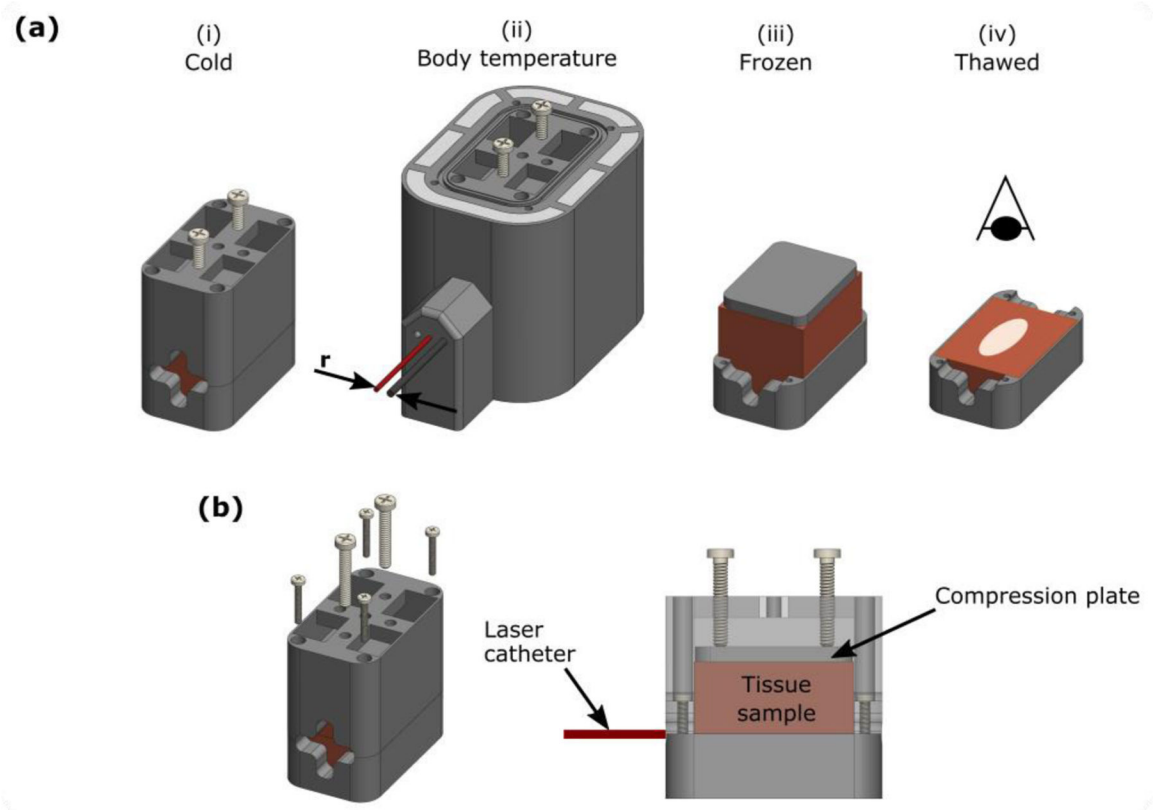

Fig. 2.

Experimental setup for ex vivo bovine muscle laser ablation. (a) The tissue sample was secured in a 3D printed sample holder (i) and then placed in a thin bag to facilitate preheating to 37°C in a water bath. Subsequently, the sample holder was transferred to an insulated testing rig (ii) with needle tracks designed to ensure accurate separation of the laser catheter and optical probe (r). To ensure precise sectioning along the trajectory of the laser fiber, the sample was frozen overnight. The top section of the sample holder was then removed (iii) and the sample was sliced along the surface of the remaining bottom section (iv). The sample was allowed to thaw before being photographed in a lightbox. (b) Detailed view of tissue sample holder. Note that the sample is compressed to reduce tissue pliability and ensure the laser track remains in plane with the edge of the bottom section of the sample holder.

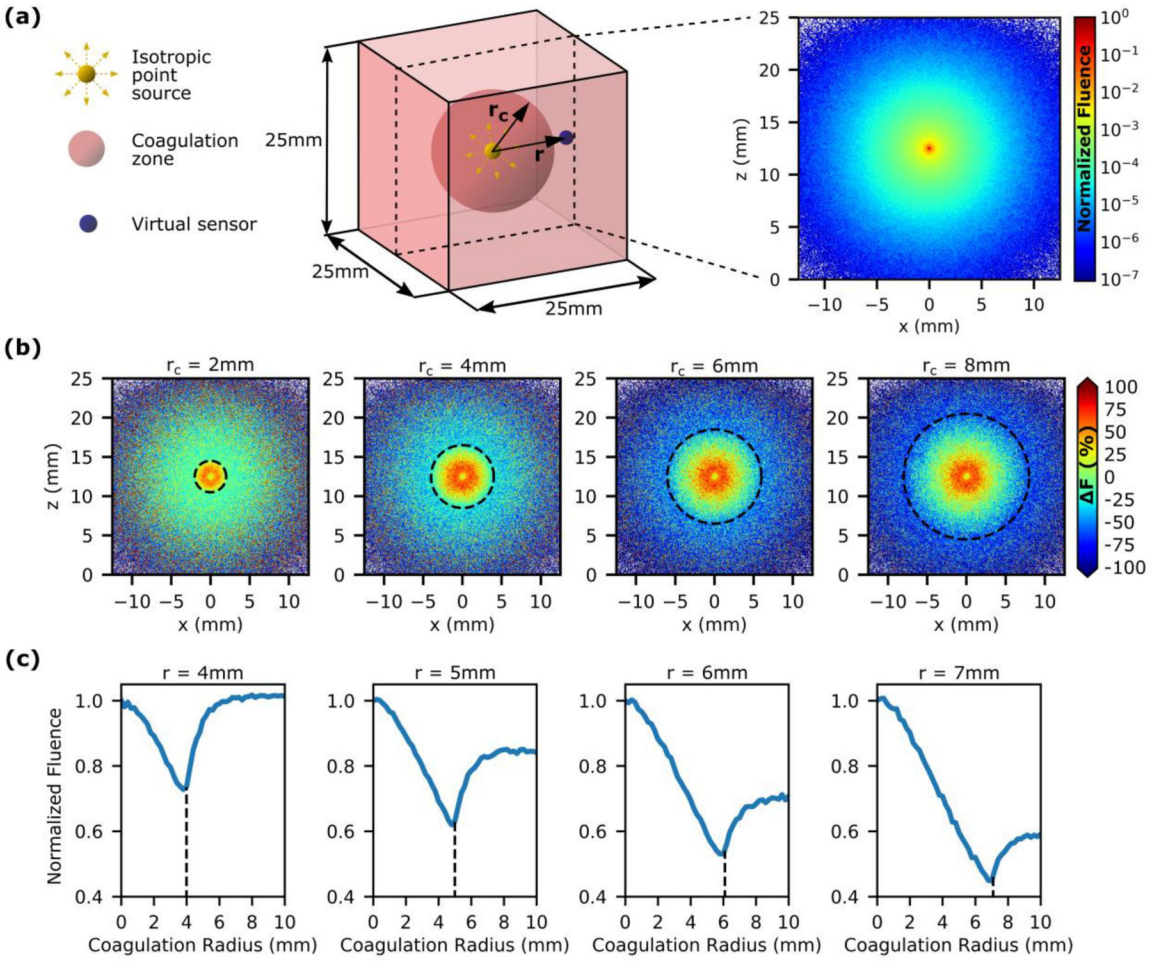

Fig. 3.

Analysis of laser-tissue interaction during FLA in prostatic tissue with a Monte Carlo model. (a) Setup for Monte Carlo simulation with a single isotropic point source at the center of a spherical coagulation zone (left). Fluence distribution before the onset of coagulation (right). (b) The change in fluence (ΔF) due to the outward expansion of the coagulation zone (dashed line indicates coagulation boundary). (c) The effect of the growing coagulation zone on the fluence recorded by virtual sensors located at distances (r) 4–7mm from the isotropic point source. An inflection point is observed as the coagulation boundary passes the virtual sensor (dashed line). This suggests that it may be possible to achieve pre-defined ablation zones clinically by positioning an optical sensor at the desired ablation boundary and terminating energy exposure once the inflection point is observed.

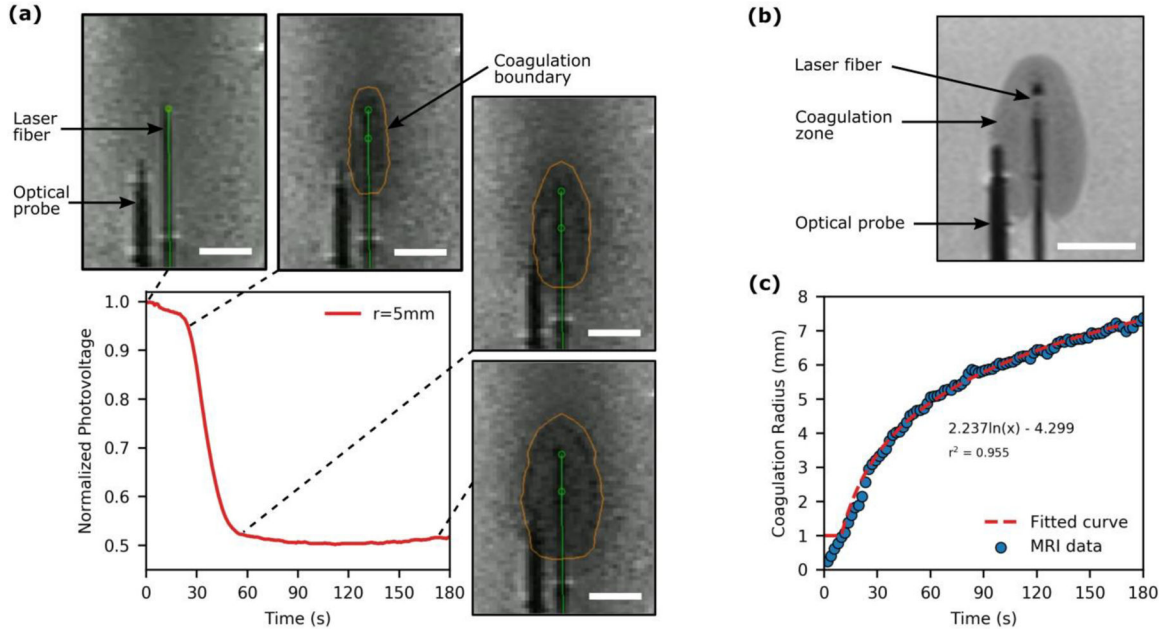

Fig. 4.

Analysis of laser-tissue interaction during FLA in a tissue-mimicking phantom under simultaneous MRI surveillance. (a) The acquired optical signal and corresponding MRI images (INTRA) for FLA with the ballistic probe positioned 5mm from the laser fiber. The optical signal decreases as the coagulation zone expands towards the probe with an inflection point observed once the coagulation zone reaches the probe. (b) A high-resolution MRI (POST) acquired immediately after FLA. (c) An example of the growth of the coagulation radius as a function of time which was described with a logarithmic function to facilitate temporal resolution with the acquired photovoltage data. [All scale bars are 10mm]

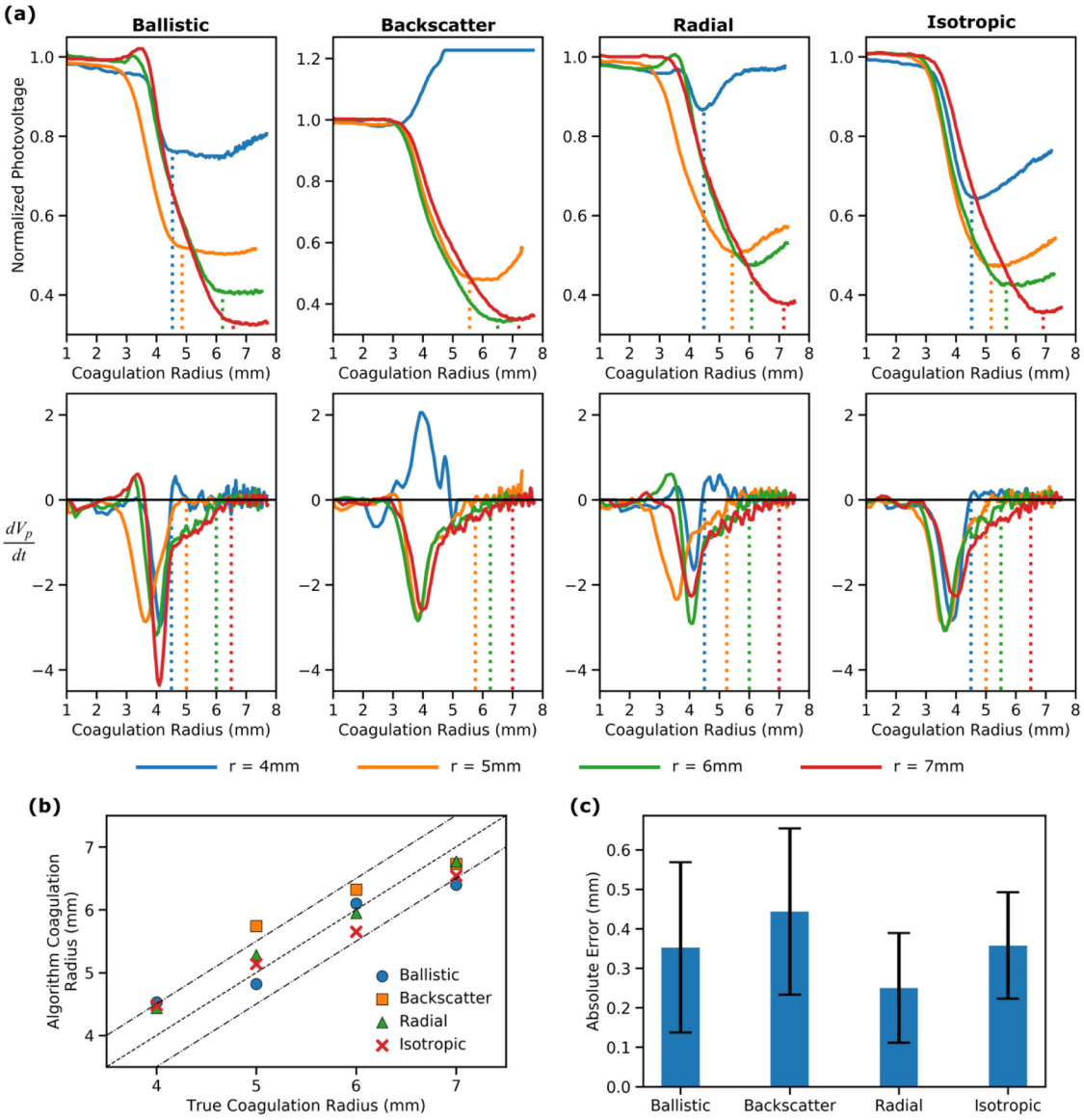

Fig. 5.

A comparison of the utility of different interstitial optical probes for monitoring FLA. (a) Top row: Normalized photovoltage vs coagulation radius (r_c) for each probe at each probe-laser fiber separation distance (r). The dashed lines indicate when the instantaneous rate of change (dV_p/dr_c) returns to zero. Bottom row: Instantaneous rate of change of the photovoltage with respect to time (dV_p/dt) vs coagulation radius. The dashed lines indicate where the instantaneous rate of change returns to zero after reaching its minimum value. (b) The coagulation radius retrospectively identified by an algorithm capable of analyzing the optical data in real-time vs the true coagulation radius from the MRI data. The dashed lines represent the line of equivalence ± 1mm. (c) The error (difference between desired coagulation radius and true coagulation radius) that would have occurred if the algorithm was used to inform the decision to terminate laser exposure. Error bars are ± one standard deviation.

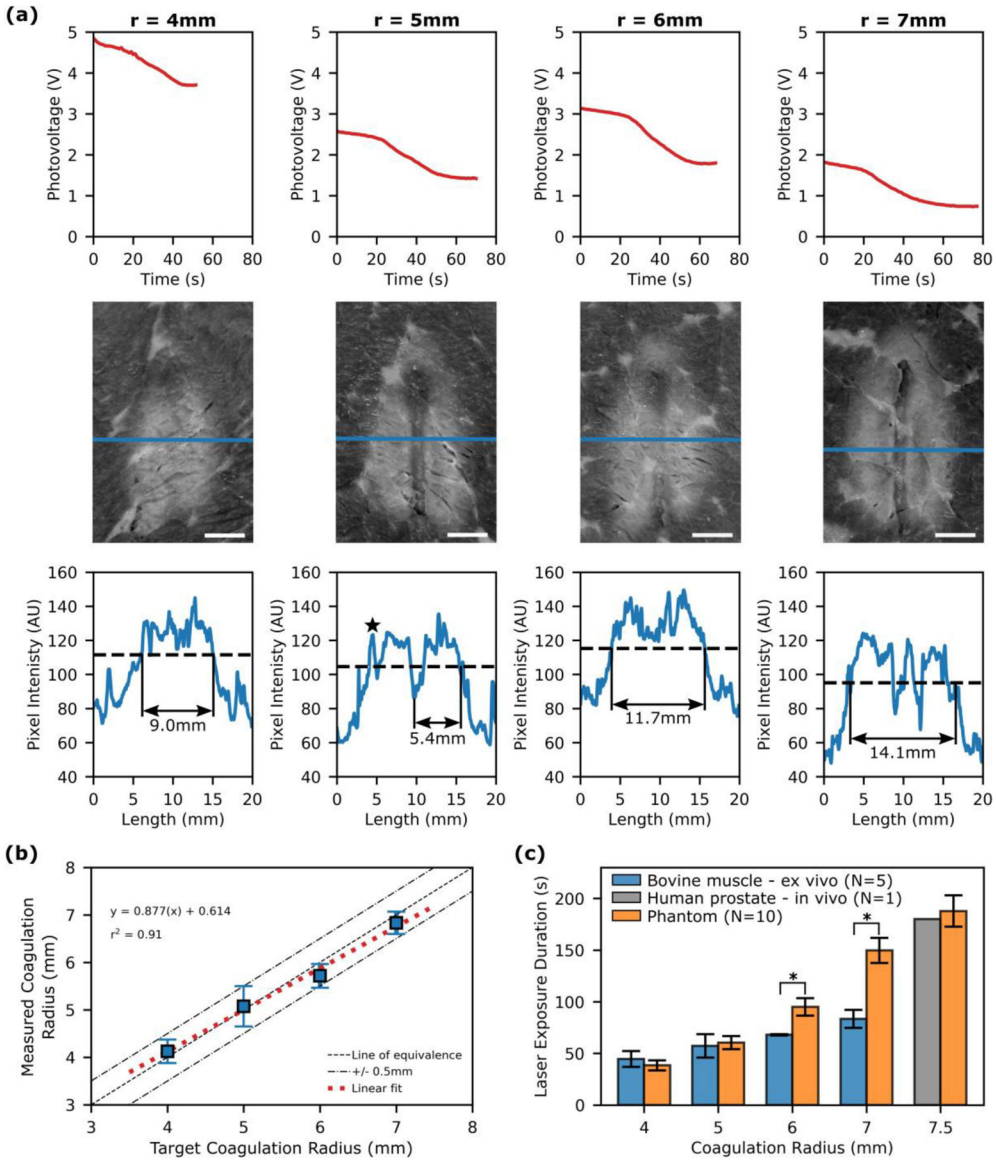

Fig. 6.

Interstitial optical monitoring of FLA in ex vivo bovine muscle. (a) Each column contains the data acquired when attempting to achieve a desired ablation radius (r) in ex vivo bovine muscle. Top - Photovoltage recorded by the FLA monitoring software and analyzed in real-time using the feedback algorithm to inform the decision to terminate laser exposure. Middle - photograph of the resulting ablation zone. Note the profile line (blue) defined by the user during image analysis. Bottom - profile lines (blue) and coagulation threshold (dashed line) used to determine the coagulation radius by measuring the diameter. Note that for r=5, fat obscures the left edge and is seen as a signal spike on the profile line (black star). In this case the radius is measured from the center of the dual lumen catheter track. [Scale bars are 5mm]. (b) Comparison of the measured radius with the target damage radius. (c) The exposure duration required to achieve different ablation sizes in bovine muscle, tissue mimicking phantom and human prostate. [* $p < 0.01$, Wilcoxon rank-sum test]

Table 1.

Turbo spin-echo MRI sequence parameters for dynamic intra-procedural scans (INTRA) and higher-resolution pre- and post-ablation scans (PRE/POST). These scans were custom designed in-house to facilitate imaging of focal laser ablation in the tissue mimicking phantom. Note that the temporal resolution of the INTRA scan is increased by sacrificing both spatial resolution and contrast to noise ratio.

Scan Type	TE (ms)	TR (ms)	Echo Train Length	Duration (s/image)	Pixel Size (mm^2)	Slice Thickness (mm)
INTRA	16	390	13	2	0.75*0.75	2
PRE/POST	52	2000	13	47	0.5*0.5	1

IEEE Trans Biomed Eng. Author manuscript; available in PMC 2023 August 01.